RSC Advances

PAPER

View Article Online
View Journal | View Issue

Cite this: *RSC Adv.*, 2022, **12**, 8578

Theoretical design and characterization of new terpolymer donors based on PTB7Ir for high-efficiency triplet-material-based organic photovoltaics†

Shuangbao Li, *[a] Yang Chen,[a] Zhen Li, [a] Jianpo Zhang,[a] Jie Chen, [a] Yun Geng [b] and Zhongmin Su *[bcd]

In the current work, eleven terpolymer donors with different electron-withdrawing groups were designed and investigated based on the reported **PTB7Ir** to screen outstanding donors for triplet-material-based organic photovoltaics (T-OPVs). Geometry structures, frontier molecular orbital energy levels, energy driving forces (ΔE_{L-L}), absorption spectra, energy differences between S_1 and T_1 states (ΔE_{ST}), and driving forces of the triplet charge recombination ($-\Delta G_{CRT}$) of **PTB7Ir** and designed **1–11** systems were evaluated by DFT and TD-DFT methods to estimate the light absorption abilities and the charge transfer dynamics. The results show that designed **5**, **8**, **10** and **11** possess larger spin–orbit couplings (SOC) affinity and smaller ΔE_{ST} and $-\Delta G_{CRT}$ values, which could effectively suppress the triplet charge recombination process at the donor/acceptor interface. Excitingly, the designed terpolymer **10** presents enhanced light absorption, revealing that it will be a promising donor candidate for high-performance T-OPV devices. Moreover, the results can provide theoretical guidelines to predict new terpolymer donors of T-OPVs.

Received 4th January 2022
Accepted 15th March 2022

DOI: 10.1039/d2ra00033d

rsc.li/rsc-advances

1. Introduction

Organic photovoltaics (OPVs) have achieved impressive advances in their low-cost fabrication, large-area production, and flexible device structure.[1–5] To date, favorable power conversion efficiencies (PCEs) of over 18% have been obtained,[6–9] which make the industrialization possible. The exploration of high-efficiency photovoltaic materials in OPVs has been regarded as one of the significant challenges for improving the PCE.

In OPV devices, excitons are photogenerated in donor (D) and/or acceptor (A) species and dissociated at D/A interfaces. This process leads to either direct long-range charge separation or generation of interfacial singlet charge transfer (^{1}CT) states followed by vibrational relaxation to the lowest ^{1}CT ($^1CT_1$) states. Then the interfacial $^1CT_1$ states dissociate into free charge carriers, but also can occur geminate charge recombination (CR) which competes with exciton dissociation.[10] In order to achieve a high-efficiency solar cell device, it is necessary to restrain geminate CR processes. One effective way is to promote the generation of triplet charge transfer (^{3}CT) states. On one hand, triplet excitons can provide sufficient time for the CT state to dissociate the bound charge pair rather than recombination, because their radiative decay is dipole forbidden which will lead to longer lifetimes.[11,12] On the other hand, it is found that the charge transfer from the lowest charge transfer triplet ($^3CT_1$) to triplet excited (T_1) states, *i.e.*, the charge recombination to triplet (CRT), can be prevented when the energy level of ^{3}CT state is lower than that of T_1 state of donor materials.[13,14] The state diagram of various photophysical processes is shown in Fig. 1.

In order to get more ^{3}CT states, triplet materials containing heavy metal complexes are adopted as source of ^{3}CT by some research groups, and leading to the increased charge-transfer efficiency and improved photovoltaic performance.[11,12,15–20] Notably, Huang and co-workers reported a series of Ir-

[a]*School of Chemical and Pharmaceutical Engineering, Jilin Institute of Chemical Technology, Jilin, 132022, P. R. China. E-mail: lishb997@nenu.edu.cn*

[b]*Institute of Functional Material Chemistry, Faculty of Chemistry, Northeast Normal University, Changchun, 130024, P. R. China*

[c]*School of Chemistry and Environmental Engineering, Changchun University of Science and Technology, Changchun, 130022, P. R. China*

[d]*Jilin Provincial Science and Technology Innovation Center of Optical Materials and Chemistry, Changchun, 130022, P. R. China*

† Electronic supplementary information (ESI) available: A comparative analysis of intermolecular charge transfer properties of **PTB7Ir**/$PC_{71}BM$ based on the ground-state geometries calculated by PBE0 and PBE0-D2 functionals, respectively. The plots of schematic illustration of twist angles between donor and acceptor moieties of **2** and **6–11**, and hole–electron pairs of NTOs in S_1 and T_1 states of **1–3** and **5–11**. The tables of HOMO energy levels (E_{HOMO}) calculated using B3LYP functional, and the vertical excitation energies (E_g), oscillator strengths (f) and excitation characters of S_1 states calculated at the B3LYP/6-31G(d) (LANL2DZ for Ir atom) level in *o*-dichlorobenzene solvent for **PTB7Ir** and **1–11** molecules. Tables of coordinates of molecules. See DOI: 10.1039/d2ra00033d

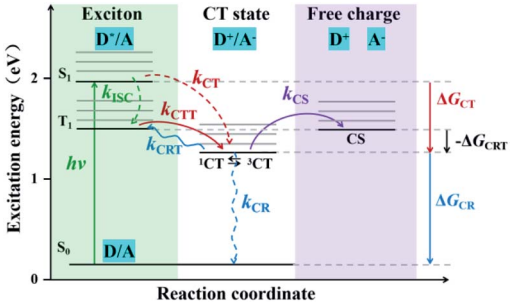

Fig. 1 State diagram of various photophysical processes in the case of "donor" excitation for T-OPVs. Charge transfer (CT) and charge separated (CS) state energies are shown in relation to the first singlet excited state (S_1), the first triplet excited state (T_1) and ground state (S_0). Excitons are photogenerated in donors and dissociated at D/A interfaces, when CT energy below the T_1 state, photoexcited excitons go through a fast intersystem crossing (ISC) from S_1 to T_1 states at a rate k_{ISC} (green dotted arrow), then the ^{3}CT states are formed from the T_1 at a rate k_{CTT} (red arrow), and finally separated into free charges at a rate k_{CS} (purple arrow); also, one possibility even in the triplet system, ^{1}CT excitons may generate from S_1 without going through T_1 at a rate k_{CT} (red dotted arrow). In addition, when CT energy above the T_1 state, the ^{1}CT states are formed directly from S_1 (red dotted arrow), yielding the ISC from ^{1}CT to ^{3}CT, and thus the ^{3}CT state separated into free charges. It's worth noting that there can occur the triplet charge recombination (CRT) from ^{3}CT to T_1 at a rate k_{CRT} (blue arrow). ΔG_{CT}, ΔG_{CR} and $-\Delta G_{CRT}$ refer to the driving forces of CT, CR and CRT, respectively.

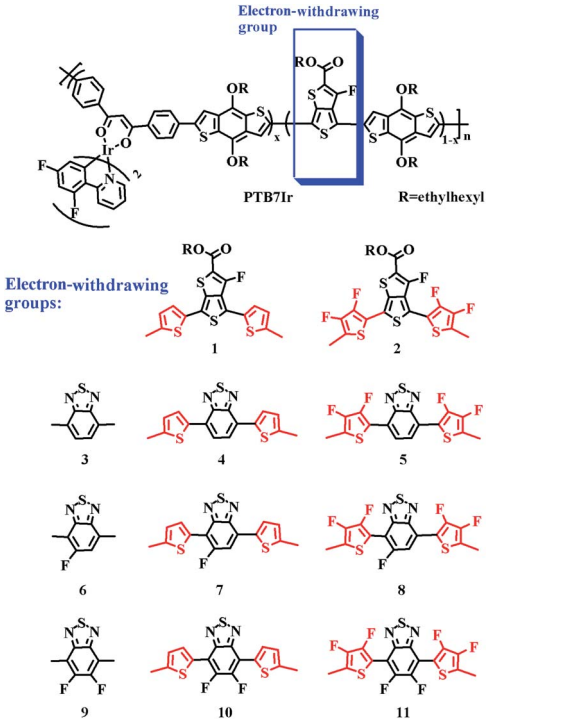

Fig. 2 Molecular structures of **PTB7Ir** and **1–11**. Among, the defined electron-withdrawing group contains π-bridge, *x* represents the various ratio of $(dfppy)_2Ir(dbm)$ complex, and *n* represents the number of repeating units.

embedded **PTB7Ir** polymers (see in Fig. 2), in which various low concentrations of $(dfppy)_2Ir(dbm)$ (0–5 mol%) were introduced into the backbone of PTB7 (polythieno[3,4-*b*]-thiophene-*co*-benzodithiophene), and the improved PCEs have been achieved owing to the participation of triplet effects. Compared to PTB7, the PCEs of the devices based on **PTB7Ir1** (containing 1 mol% Ir concentration) were all enhanced over 30%.[12] In addition, they introduced a low concentration of Pt/Ir complexes into the PTB7-Th polymer backbone (it is made by grafting the 2-ethylhexyl-thienyl group into the benzodithiophene unit of PTB7) by a similar approach, achieving the increases of PCEs from 7.92% to 8.45% and 9.19%, respectively.[19,20] However, so far, there are no explicit design strategies of terpolymer donors containing heavy metal complexes of triplet material-based OPVs (T-OPVs), because it is difficult to build a direct relationship between photoelectric conversion efficiency and molecular structure of the donor or D/A complex. Previously, we explored why **PTB7Ir**/$PC_{71}BM$ device exhibits the enhanced PCE (8.71%) compared with 6.64% of PTB7/$PC_{71}BM$ device, and discussed how to prevent the CRT process at D/A interface for T-OPVs.[21] The results indicate that the improved PCE of the **PTB7Ir**/$PC_{71}BM$ device is mainly ascribed to the increasing exciton diffusion length of triplet excitons. Besides, the proper increase of angle and number of torsional angles between electron donating and withdrawing units of terpolymer donors can prevent the CRT process and further improve photovoltaic performance.

Herein, in the basis of **PTB7Ir**, we designed eleven terpolymers **1–11** through modifying and replacing the electron-withdrawing acceptor groups of **PTB7Ir**. All repeated units of **PTB7Ir** and terpolymers **1–11** are shown in Fig. 2. The introductions of thiophene π-bridge, fluorinated thiophene π-bridge, benzothiadiazole (BT) group and fluorinated benzothiadiazole (FBT and DFBT) group are aimed at tuning the energy levels and energy-gaps of S_1, T_1 and CT_1 states to improve the short-circuit current density (J_{sc}). For example, (i) reducing the S_1 energy level to broaden absorption spectra in near infrared range; (ii) reducing the energy difference between S_1 and T_1 states to promote intersystem crossing (ISC) process of excitons from singlet to triplet; and (iii) tuning $^3CT_1$ energy level lower than T_1 energy level to decrease values of driving force for the CRT ($-\Delta G_{CRT}$) as well as prevent CRT process. By density functional theory (DFT) and time-dependent DFT (TD-DFT) methods, we systematically investigated geometry structures, frontier molecular orbital (FMO) energy levels, energy driving forces (ΔE_{L-L}), absorption spectra, energy differences between S_1 and T_1 states (ΔE_{ST}), and $-\Delta G_{CRT}$ of **PTB7Ir**/$PC_{71}BM$ and **1–11**/$PC_{71}BM$ systems, to perform a further analysis on charge transfer properties for efficient charge separation and photocurrent generation in T-OPVs. We expect that this work may serve as a theoretical guideline for the design and synthesis of high-performance T-OPV terpolymer donors.

2. Computational details

It has been reported that alkyl-branched chains possess little influence on the electronic structures and photoelectric

properties of materials.[22–24] Therefore, for all investigated polymers, the branched ethylhexyl side chains were substitute by methyl groups and the ends of oligomers were capped by hydrogen atoms to save computational cost. All of the calculations were performed by using Gaussian 09 software.[25] Ir atom and non-metal atoms were described by LANL2DZ basis set and 6-31G(d) basis set, respectively.

In our previous research,[21] it is confirmed that when **PTB7Ir** molecule contain one metal complex and three organic building blocks ($x = 0.25$), the calculated HOMO energy level by PBE0 functional show good accordance with the measured experimentally (the calculated HOMO level is −5.16 eV and experimental values are in the range of −5.14 to −5.22 eV).[12] Additionally, the B3LYP functional was proved to be an effective method to evaluate the absorption spectrum and the S_1 vertical excitation energies of **PTB7Ir** molecule, because the maximum absorption wavelength value of **PTB7Ir** molecule calculated by TD-B3LYP//PBE0 functional (672 nm) is closer to the experimental data (678 nm).[21] Meanwhile the effect of solvent (*o*-dichlorobenzene (DCB)) within polarizable continuum model (PCM) was considered in TD-DFT calculations. Also, the HOMO–LUMO energy gap of **PTB7Ir** was estimated as S_1 vertical excitation energy, and the LUMO energy level was derived by adding the band-gap to HOMO level. The result from this method agreed well with the experimental LUMO level (the calculated LUMO energy level is −3.29 eV, electronic energy level is −2.70 eV, and experimental values are −3.02 to −3.13 eV).[12] Thus, in this work, the above calculated methods were employed to investigate the geometries, FMO energy levels and photoexcitation properties of all terpolymer molecules. The calculation details are listed as follows: (i) ground-state geometries and HOMO energy levels are simulated by PBE0 functional; (ii) the absorption spectra, S_1 and T_1 vertical excitation energies are evaluated at the TD-PCM-B3LYP//PBE0 level in DCB solution; and (iii) the LUMO energy levels are obtained by adding S_1 vertical excitation energies to the HOMO energy levels.

Our previous results indicated that when $PC_{71}BM$ is docked with the centre of polymer donor, the interfacial arrangement is preferable for **PTB7Ir**/$PC_{71}BM$ complex, since the lowest energies occur at the configuration.[21] Therefore, in current work, for each D/$PC_{71}BM$ interface model, the starting configuration is designated that benzene cycle of $PC_{71}BM$ is oriented parallel to the thiophene (for **PTB7Ir**, **1** and **2** molecules) or benzene (for **3–11** molecules) cycles of acceptor units which are closer to the $(dfppy)_2Ir(dbm)$ complexes, which has been proved to be a preferred interfacial arrangement in our previous research. The initial distances between terpolymer donors and $PC_{71}BM$ were fixed at 3.5 Å. To save the computational cost, we demonstrated a comparative analysis of intermolecular charge transfer properties of **PTB7Ir**/$PC_{71}BM$ based on the ground-state geometries calculated by PBE0 and PBE0-D2 functionals, respectively (see Section SI of the ESI†). Note that PBE0-D2 is a functional considering dispersion correction, which presents the high computational cost. The results indicate that the two interface configurations of **PTB7Ir**/$PC_{71}BM$ exhibit similar equilibrium geometries and intermolecular charge transfer behaviors. Therefore, ground-state geometries of D/$PC_{71}BM$ complexes can be performed by PBE0 functional instead of PBE0-D2 functional with dispersion correction. Excited state properties were performed at the long-range-corrected CAM-B3LYP[26,27] levels. It has been confirmed that CAM-B3LYP functional is suitable for the description of CT excited state properties of interfacial systems.[28–30] The charge density difference (CDD) maps were simulated using Multiwfn 3.3.8 code[31,32] to visualize CT excited states.[33,34]

3. Results and discussions

3.1 3D geometries

All molecular geometries were optimized at the PBE0 level as the above methods. The computed twist angles between each building blocks of **PTB7Ir** and **1–11** are plotted in Fig. 3 and S3 in ESI.† As seen from Fig. 3, twist angles between donor (benzothiadiazole, BDT) and acceptor (fluorinated benzothiadiazole, F-TT) units of **PTB7Ir** are in the range from 15° to 32°. Compared with **PTB7Ir**, the designed **1** and **2** show planar molecular structures due to the introductions of thiophene and fluorinated thiophene π-bridges. In particular, for **2** (see Fig. S3†), the twist angles between organic building blocks are all in close to 0° because of intramolecular F···S attractive interactions. And the distances between F and S atoms are approximately 2.92 Å, which are shorter than the sum of F and S van der Waals radii (3.27 Å proposed by Bondi and 3.19 Å proposed by Pauling). The planar molecular structures in the

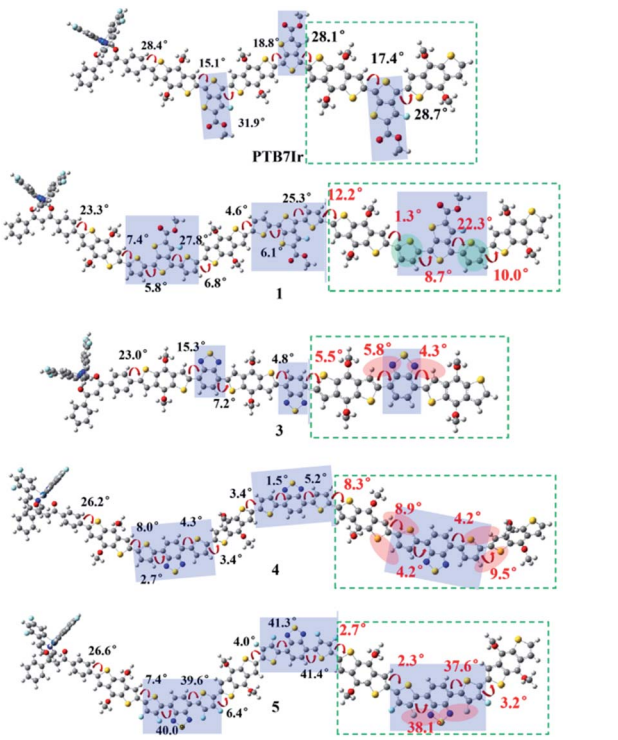

Fig. 3 Schematic illustration of twist angles between donor and acceptor moieties of PTB7Ir, 1 and 3–5. The green dotted boxes represent the highlights.

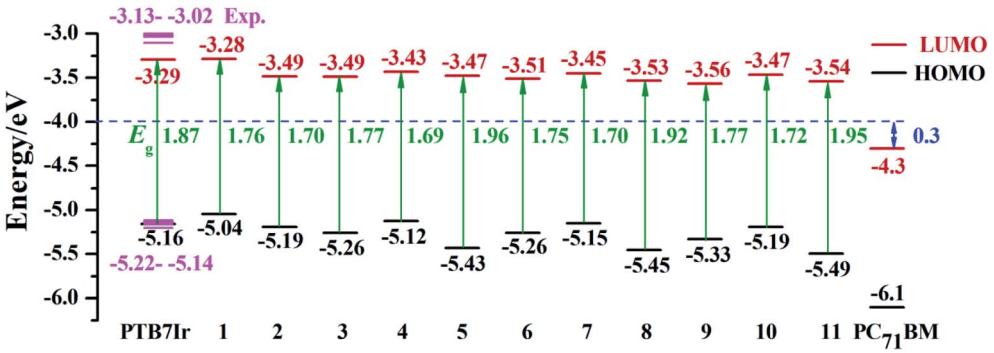

Fig. 4 Calculated FMO energy levels and S_1 vertical excitation energies (E_g) of **PTB7Ir** and **1–11** (the pink color represents the experimental value of **PTB7Ir**), along with the FMO energy level of $PC_{71}BM$ measured in experiment.

conjugated backbone increase more efficient π delocalization along the polymer chain, which will favor π-stacking and charge-transport properties. Compared to **PTB7Ir**, the designed **3**, **6** and **9** also present increasing planarity due to the attractive interactions between N atom from benzothiadiazole and H atom from BDT, respectively. Obviously, **6** and **9** show perfect planar constructions, and the optimized twist angles between BDT and acceptor units (FBT for **6** and DFBT for **9**) are also about 0°, which is attributed to N···H and F···S attractive interactions. In addition, compare with **PTB7Ir**, **4**, **5**, **7**, **8**, **10** and **11** adopt more twisted conformation, which may decrease the conjugation extent of polymers and increase the energy levels of S_1 and T_1 states. When T_1 energy above the CT_1 state, the CRT at D/A interface will be prevented to improve photovoltaic performance. However, note that the less planarity will cause the limited π-stacking interactions and lead to the undesirable

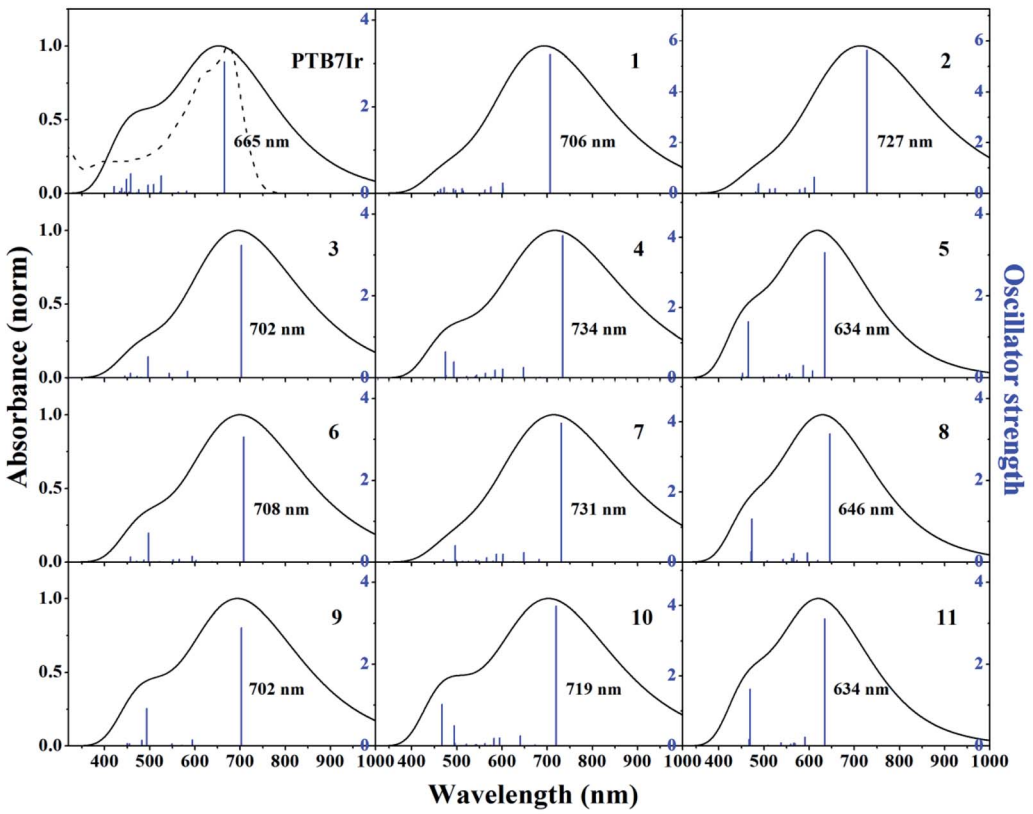

Fig. 5 Simulated absorption spectra and oscillator strengths of **PTB7Ir** and **1–11** at the TD-PCM-B3LYP/6-31G(d) (LANL2DZ for Ir atom) level. The dotted line is the experimental absorption spectrum of **PTB7Ir**. Gaussian function was chosen as the broadening function with the value of the full width at half maximum set at 0.66667 eV, which is considered as an average width for the absorption band observed in the UV-vis region.[44]

charge transport and collection. Specifically, **4** present decreasing planarity in comparison with that of **3**, which is because the repulsive interactions between H atom from thiophene π-bridge (or BDT) unit and S atom from BDT (or thiophene π-bridge) unit. Similarly, the planarity of **7** and **10** is lower than those of **6** and **9**, respectively, because of the introduction of thiophene π-bridge. Unexpectedly, for **5**, **8** and **11**, the significant repulsive interactions, between F atom from fluorinated thiophene π-bridge and N atom from benzothiadiazole, lead to twist angles of ~40° in the polymer backbone. As a result, the designed **1–3**, **6** and **9** could display better charge transport and collection owing to their improved planarity, meanwhile, **4**, **7** and **10** may suppress the CRT at the interface and enhance photovoltaic performance due to the proper torsional angles.

3.2 FMO energy levels

It is well known that FMO energy levels can dominate the photon absorption and charge separation abilities of OPVs.[35,36] The FMO energy levels of all terpolymers are listed in Fig. 4, which are obtained according to the description of calculation details in Section 2. Also, the HOMO energy levels (E_{HOMO}) calculated at the B3LYP/6-31G(d) (LANL2DZ for Ir atom) level are displayed in Table S2 in ESI.† Additionally, the FMO energy levels of the acceptor $PC_{71}BM$ measured in experiment are also depicted in Fig. 4.[37,38] Seen from Fig. 4, the energy-gap (HOMO–LUMO) values of **5**, **8** and **11** are larger than that of **PTB7Ir**, indicating that they may exhibit blue-shifted absorptions in comparison with **PTB7Ir**. This is because the significant twist angles in polymer backbones decrease the effective conjugation lengths.

The energetic driving force ΔE_{L-L}, defined by the difference between LUMO levels of donor and acceptor, is an important factor to evaluate charge separation ability at D/A interface.[28,39] The charge separation of polymers will occur when ΔE_{L-L} > 0.3 eV which is the estimated value of empirical exciton binding energy for polymers.[37,40] As seen from Fig. 4, the calculated ΔE_{L-L} values of all systems are larger than 0.3 eV, revealing the efficient charge separation at D/A interface.

3.3 Photon absorption

It is acknowledged that absorption spectra of donors need match the solar spectrum to ensure the efficient photovoltaic conversion, which will increase the J_{sc} and thus improve the PCE.[41–43] The absorption spectra of **PTB7Ir** and **1–11** are shown in Fig. 5. Vertical excitation energies, oscillator strengths and dominant configurations of S_1 states, and electronic density contours of FMOs are gathered in Tables S3† and 1, respectively. Seen from Fig. 5, the absorption range of all molecules cover the entire ultraviolet-visible, and the designed **3–11** display the similar peak shape and intensity in comparison with **PTB7Ir**. In addition, compared with **PTB7Ir**, the designed **5**, **8** and **11** exhibit slightly blue-shifted absorption in low-energy region. This is because the introduction of fluorinated thiophene π-bridges brings about their large twist angles, which lead to poor conjugation along polymer backbones. Fortunately, other designed molecules have broadened and red-shifted absorption in the 400–1000 nm region. Table S3† illustrates that the maximum absorption peaks of all systems come from $S_0 \rightarrow S_1$, corresponding to the transition from HOMO (H) to LUMO (L). The orbitals in HOMOs are mainly delocalized on the organic building blocks of polymers. Also, for **PTB7Ir**, the distribution of LUMO is localized on all organic building blocks (Table 1). For designed **3**, **6** and **9**, LUMO orbitals are mainly localized the

Table 1 Calculated electronic density contours of FMOs for **PTB7Ir** and **1–11** at the TD-PCM-B3LYP/6-31G(d) (LANL2DZ for Ir atom) level. The orbitals are plotted at a contour value of 0.01 a.u

Molecule	HOMO	LUMO
PTB7Ir	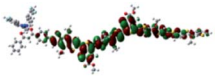	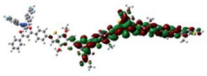
1	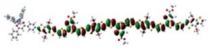	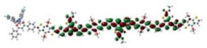
2	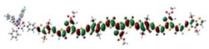	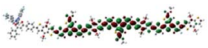
3		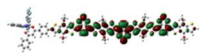
4	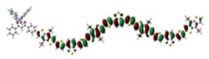	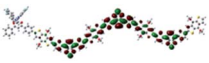
5		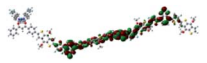
6		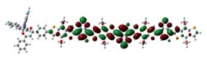
7	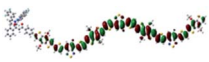	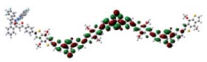
8		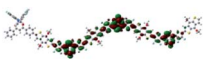
9		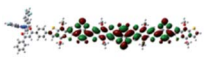
10	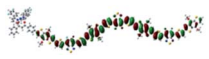	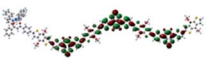
11	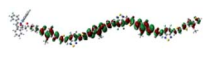	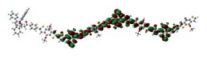

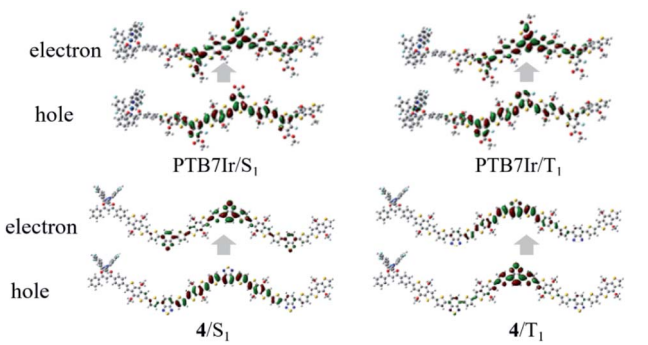

Fig. 6 Hole–electron pairs of NTOs in S_1 and T_1 states of **PTB7Ir** and **4**.

Table 2 Calculated energy level values of S_1, T_1 and ΔE_{ST} for **PTB7Ir** and **1–11** systems

	PTB7Ir	**1**	**2**	**3**	**4**	**5**	**6**	**7**	**8**	**9**	**10**	**11**
S_1/eV	**1.87**	**1.76**	**1.70**	**1.77**	**1.69**	**1.96**	**1.75**	**1.70**	**1.92**	**1.77**	**1.72**	**1.95**
T_1/eV	1.28	1.19	1.15	1.23	1.16	1.50	1.25	1.20	1.48	1.28	1.24	1.53
ΔE_{ST_1}/eV	0.59	0.57	0.55	0.54	0.53	0.46	0.50	0.50	0.44	0.49	0.48	0.42

middle three BDT units and three organic acceptor units. For other designed molecules, LUMO orbitals are localized the second and third BDT units from right, π-bridges, and organic acceptor units. The results indeed show that the designed **1–3**, **4**, **6**, **7**, **9** and **10** will present enhanced light absorption owing to their broad and red-shifted absorption in the visible and near-infrared regions of the solar spectrum.

3.4 Energy difference between S_1 and T_1 states

In T-OPVs, photoconversion channel that we are mainly concerned about is the CRT process, which can be estimated from the state diagram with measured/calculated relative energetic positions of S_1 and T_1 on the donor material and the CT_1 at the D/A interface.[13,45] Therefore, our discussion focuses on energy levels of S_1, T_1 and CT_1 rather than higher excited states. When $-\Delta G_{CRT} < 0$, the ^{3}CT excitons from T_1 or/and ^{1}CT from S_1 excitons would diffuse toward D/A interface to dissociate into separated charges.[21] Therefore, the ISC process from S_1 to T_1 need to be promoted to obtain more long-lived ^{3}CT excitons. It is widely accepted that a large spin–orbit coupling (SOC) and a small energy difference between S_1 and T_1 states (ΔE_{ST}) will lead to a fast ISC process. However, the SOC calculation of large systems is a difficult challenge need to be overcome. Fortunately, Brédas and co-workers have reported that the SOC matrix element can be qualitatively evaluated by estimating the changes in π-conjugation of either hole or electron wave functions between the singlet and triplet excited states, which is in accord with El-Sayed rule.[46] Therefore, the natural transition orbital (NTO) analyses for S_1 and T_1 were performed to examine the nature of the excited states and qualitatively evaluated SOC. Taking the NTOs of **PTB7Ir** and **4** molecules as examples (see Fig. 6), for **PTB7Ir** molecule, an obvious local excitation (LE) within the middle three BDT and F-TT units appears in both S_1

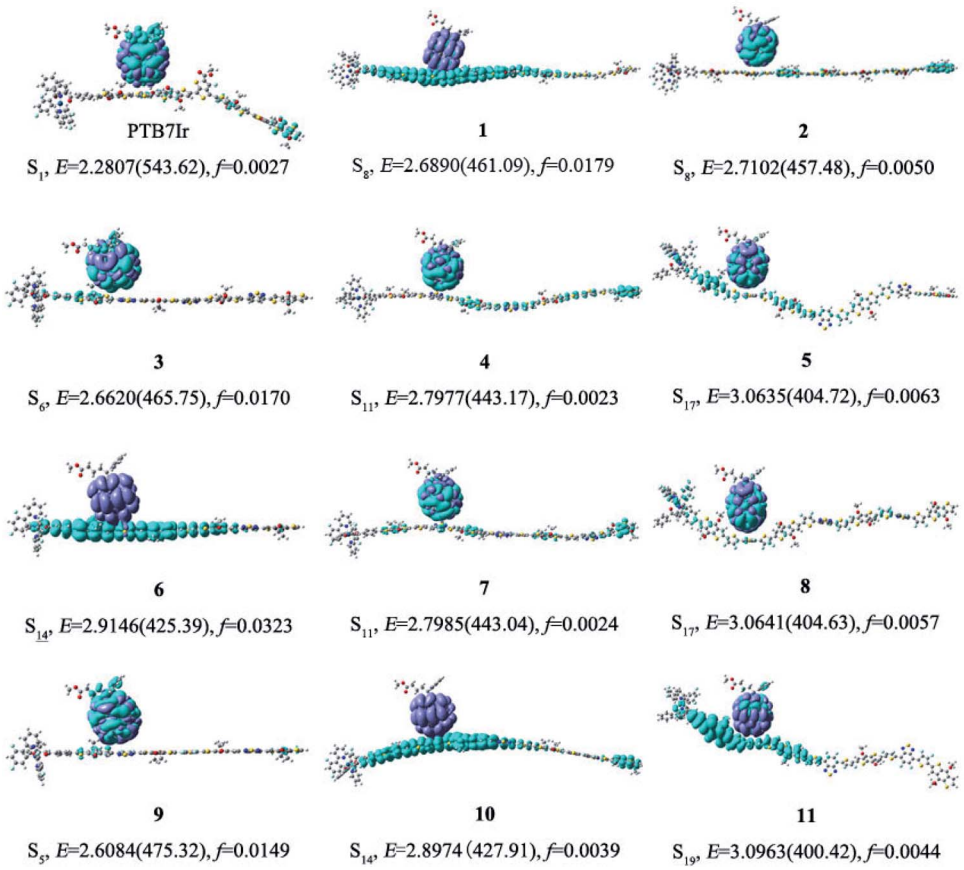

Fig. 7 CDD maps of $^1CT_1$ excited states with isosurface value of 0.00002 a.u. for **PTB7Ir**/$PC_{71}BM$ and **1–11**/$PC_{71}BM$ systems, where the violet and turquoise colors refer to the increase and decrease in electron density, respectively.

and T_1 states, which will lead to a small SOC; for **4** molecule, besides the LE character within organic acceptor units, a clear CT character from middle two BDT donor units to organic acceptor units also occurs in the S_1 state because of the spatial separation of LUMO wave function, while only LE character appears in the T_1 state, consequently, **4** molecule will exhibit a lager SOC value than **PTB7Ir** due to the change in π-conjugation between S_1 and T_1 states. Turning to **1–3**, **6**, and **9**, a predominant LE character are presented in S_1 and T_1 states (see Fig. S4†). For **5**, **7**, **8**, **10** and **11**, the LE and CT characters are both observed in S_1 states in addition to a LE character for their T_1 states. As a result, designed **4**, **5**, **7**, **8**, **10** and **11** may give the lager SOC values than others. Note that, Ir metal centers of the designed terpolymers are not involved at both S_1 and T_1 states, indicating that the SOC mainly comes from the organic parts of terpolymer systems.

Additionally, the energy difference between S_1 and T_1 states (ΔE_{ST}) values were calculated to evaluate ISC process of all systems from S_1 to T_1 states. The calculated ΔE_{ST} values are summarized in Table 2, respectively. It shows that ΔE_{ST} values of all designed molecules are smaller than that of **PTB7Ir**. Obviously, the ΔE_{ST} of **5** and **8–11** are below the value of 0.5 eV, indicating that their ISC process could be promoted to form more long-lived ^{3}CT exciton. Unfortunately, the ΔE_{ST} values of all systems are still quite large, which will be further reduced in future. Consequently, designed **5**, **8**, **10** and **11** exhibit larger SOC affinity and smaller ΔE_{ST} values than those of **PTB7Ir**, which will promote their ISC process from S_1 to T_1 states and the formation of ^{3}CT exciton.

3.5 Intermolecular charge transfer

3.5.1 Intermolecular charge transfer excited states. It is commonly accepted that the geometry of D/A interface plays an important role in the behavior of CT state.[47] To give a deep insight into the photovoltaic properties of all aforementioned terpolymers/A heterojunctions, the charge density difference (CDD) maps were calculated to investigate the charge transfer behaviors between the ground state and the lowest intermolecular CT excited state at D/A interface. The CDD maps of $^1CT_1$ and $^3CT_1$ states are shown in Fig. 7 and 8, respectively. Note that the electrons of these CT excited states are mainly confined to acceptors.[22,30,48] As displayed in Fig. 7, the $^1CT_1$ states of **1**/$PC_{71}BM$, **6**/$PC_{71}BM$ and **10**/$PC_{71}BM$ heterojunctions include charge transfer from terpolymer backbones to $PC_{71}BM$. Differently, for other heterojunctions, the $^1CT_1$ states involve $PC_{71}BM$-localized π–π* transition and electronic transitions from donors to $PC_{71}BM$. Moreover, for **5**/$PC_{71}BM$, **8**/$PC_{71}BM$ and **11**/$PC_{71}BM$ heterojunctions, Ir complexes take part in the intermolecular charge transfer from terpolymer donors to $PC_{71}BM$, because their twist structures along polymer backbones

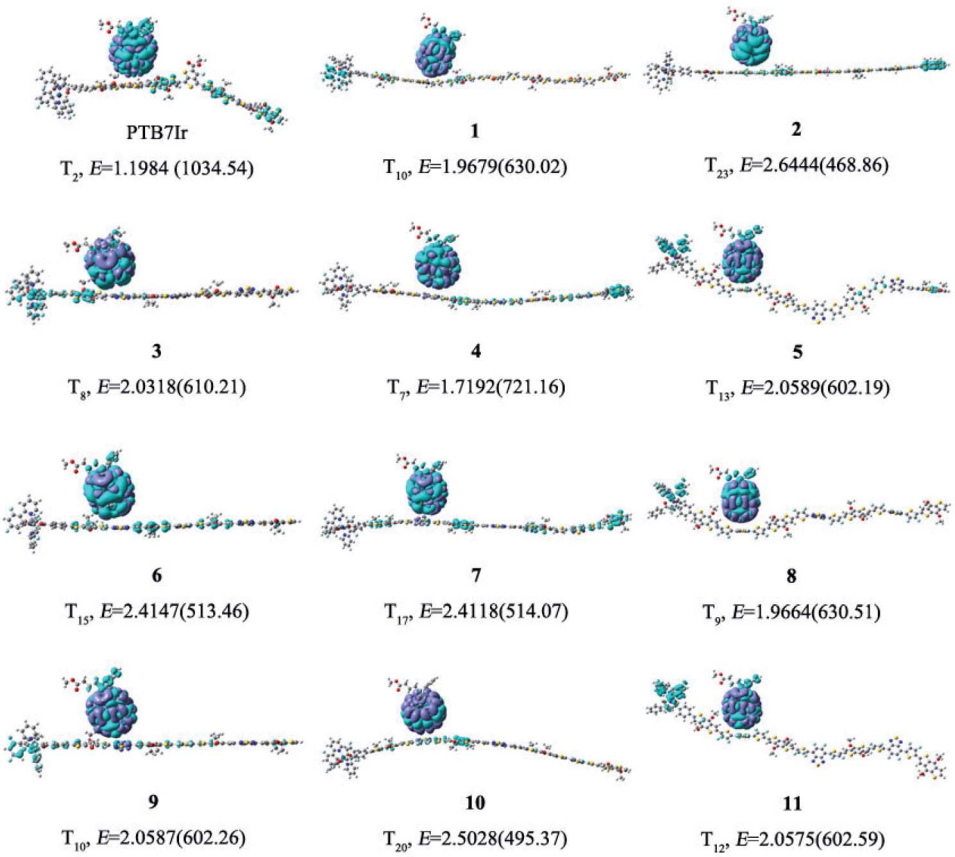

Fig. 8 CDD maps of $^3CT_1$ excited states with isosurface value of 0.00002 a.u. for **PTB7Ir**/$PC_{71}BM$ and **1–11**/$PC_{71}BM$ systems, where the violet and turquoise colors refer to the increase and decrease in electron density, respectively.

Table 3 Calculated energy level values of E_{Coul}, E_{CT_1} and $-\Delta G_{CRT}$ for **PTB7Ir** and **1–11** systems

	PTB7Ir	**1**	**2**	**3**	**4**	**5**	**6**	**7**	**8**	**9**	**10**	**11**
E_{Coul}/eV	−0.19	−0.09	−0.30	−0.15	−0.04	−0.43	−0.16	−0.19	−0.54	−0.18	−0.29	−0.69
E_{CT_1}/eV	1.22	1.12	1.05	1.28	1.25	1.17	1.27	1.13	1.08	1.32	1.07	0.97
$-\Delta G_{CRT}$/eV	−0.06	−0.07	−0.10	0.05	0.09	−0.33	0.02	−0.07	−0.40	0.04	−0.17	−0.56

increase donor–acceptor interactions *via* a decreasing in the distance between donor (mainly containing Ir complex and adjacent BDT unit) and acceptor. The increasing donor–acceptor interactions could enhance the electron–hole binding energy and result in a decrease in CT state energy.[49] Additionally, the Ir complex of **6**/$PC_{71}BM$ also involve the intermolecular charge transfer due to the short distance between Ir complex and acceptor. Likewise, the transition of $^3CT_1$ states for all heterojunctions are deemed to the charge transfer from donor polymers to $PC_{71}BM$ (Fig. 8). For **3**/$PC_{71}BM$, **5**/$PC_{71}BM$, **8**/$PC_{71}BM$, **9**/$PC_{71}BM$ and **11**/$PC_{71}BM$, the $^3CT_1$ states contain the transition from Ir complexes to $PC_{71}BM$. The results illustrate that the increasing twist angles along terpolymer backbones can promote the intermolecular charge transfer process from metal complex to acceptor and reduce CT state energy in T-OPVs.

3.5.2 Triplet charge recombination process. In T-OPVs, the charge recombination to triplet (CRT) process at the D/A interface needs to be suppressed to improve the efficiency of photocurrent generation. To illustrate the CRT process of all terpolymers, the driving force for the CRT ($-\Delta G_{CRT}$) was characterized through the energetic difference ($E_{CT_1} - E_{T_1}$) between CT_1 and T_1 states. Generally, ^{1}CT and ^{3}CT states are degenerate in energy.[44,50,51] Herein, the E_{CT_1} energy value was employed to the description of $^1CT_1$ and $^3CT_1$ energies. The energy of CT_1 state could be calculated through the equation $E_{CT_1} = |E_{IP}(D) - E_{EA}(A)| + E_{Coul}$,[13,52] in which $E_{IP}(D)$ and $E_{EA}(A)$ refer to the ionization potential of donor and the electron affinity of acceptor, which are estimated by the HOMO energy of donor and LUMO energy of acceptor, respectively.[53] E_{Coul} represents for the Coulomb interaction energy between the

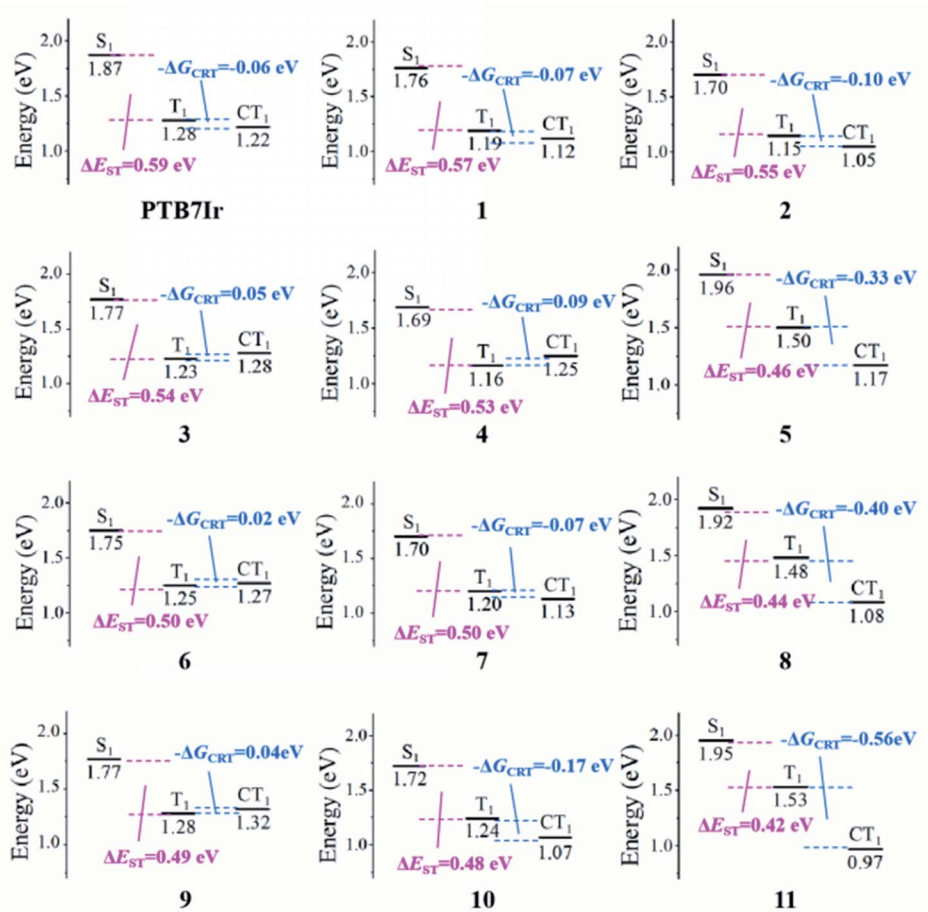

Fig. 9 Energy diagrams of the lowest singlet S_1, triplet T_1 and CT_1 charge transfer excited states relative to the ground states for the **PTB7Ir**/$PC_{71}BM$ and **1–11**/$PC_{71}BM$ heterojunctions, respectively.

cation of donor and anion of accept, which is calculated using the formula $E_{Coul}=(1/4\pi\varepsilon_0\varepsilon_r)\sum_{i\in D+}\sum_{j\in A-}(q_iq_j/r_{ij})$. Among, ε_0 and ε_r refer to dielectric constants in vacuum and medium (ε_r is set as 4.0, which refers to the experimental value reported for PTB7:$PC_{71}BM$ system[54]), respectively. q_i and q_j represent for charges of i and j atoms given by the natural population analysis charge distribution in this work, and r_{ij} is the distance between the two atoms.

The calculated energy level values of CT_1, E_{Coul} and $-\Delta G_{CRT}$ for all systems were summarized in Table 3, and energy diagrams of various states were presented in Fig. 9. As shown, the $-\Delta G_{CRT}$ values are found to be in the order of **4** > **3** > **9** > **6** > **PTB7Ir** > **1** = **7** > **2** > **10** > **5** > **8** > **11**. The result indicates that, compared with **PTB7Ir**, designed **1**, **2**, **4**, **5**, **7**, **8**, **10** and **11** exhibit smaller $-\Delta G_{CRT}$ values due to the twist donor backbones. Especially, the $-\Delta G_{CRT}$ values of **5**, **8**, **10** and **11** are less than −0.1 eV, thus leading to the suppressed CRT process. Here, the value "−0.1 eV" is considered as the minimum $-\Delta G_{CRT}$, which can give rise to the CRT process.[45] As a result, we infer that designed **10** will be a promising terpolymer donor for high-performance T-OPVs because of its broad and red-shifted absorption and suppressed CRT process at D/A interface.

4. Conclusions

To summarize, motivated by the consideration of increasing the efficiency of photocurrent generation of T-OPVs, eleven terpolymer donors have been designed and characterized based on **PTB7Ir** using DFT and TD-DFT methods. Compared to reported **PTB7Ir**, the designed **3**, **4**, **6**, **7**, **9** and **10** present broader and red-shifted absorption in the low-energy region of the solar spectrum, which contribute to capture more photons to enhance the photocurrent. Moreover, designed **5**, **8**, **10** and **11** show larger SOC affinity and smaller ΔE_{ST} values than those of **PTB7Ir**, which will promote their ISC process from S_1 to T_1 states and the formation of ^{3}CT exciton. Significantly, the $-\Delta G_{CRT}$ values of designed **5**, **8**, **10** and **11** are less than −0.1 eV, which can effectively suppress CRT process at the D/A interface. Consequently, the designed **10** possess enhanced light absorption, larger SOC affinity, smaller ΔE_{ST} and $-\Delta G_{CRT}$ values, which will be a promising candidate for terpolymer donors in high-performance T-OPVs. Meanwhile, the results manifest that the proper twist angles in terpolymer backbones could prevent the CRT process to achieve a balanced combination of charge separation, transport and collection, and further improve photovoltaic performance. Furthermore, an effective and integrated method to predict terpolymer donors embedded with metal complexes of T-OPVs is described systematically.

Author contributions

S. Li conceived the research and wrote the original draft. S. Li, Y. Chen, Z. Li, and J. Zhang performed the calculation. J. Chen, Y. Geng and Z. Su directed the research. All the authors contributed to the discussions, reviewing and editing.

Conflicts of interest

There are no conflicts to declare.

Acknowledgements

The authors gratefully acknowledge financial support from Science and Technology Project of Jilin Education Department (JJKH20200239KJ), the Fundamental Research Funds for the Central Universities (2412018ZD006), Natural Science Foundation of Jilin Province (YDZJ202101ZYTS029) and Special Training Project for Outstanding Young Talents of Jilin City (20210103092).

Notes and references

1 K. Jiang, J. Zhang, Z. Peng, F. Lin, S. Wu, Z. Li, Y. Chen, H. Yan, H. Ade, Z. Zhu and A. K. Y. Jen, *Nat. Commun.*, 2021, **12**, 468.
2 L. Zhu, M. Zhang, W. Zhong, S. Leng, G. Zhou, Y. Zou, X. Su, H. Ding, P. Gu, F. Liu and Y. Zhang, *Energy Environ. Sci.*, 2021, **14**, 4341–4357.
3 M. Jeong, J. Oh, Y. Cho, B. Lee, S. Jeong, S. M. Lee, S.-H. Kang and C. Yang, *Adv. Funct. Mater.*, 2021, 202102371.
4 G. J. Hedley, A. Ruseckas and I. D. W. Samuel, *Chem. Rev.*, 2017, **117**, 796–837.
5 K. A. Mazzio and C. K. Luscombe, *Chem. Soc. Rev.*, 2015, **44**, 78–90.
6 Y. Cui, H. Yao, J. Zhang, K. Xian, T. Zhang, L. Hong, Y. Wang, Y. Xu, K. Ma, C. An, C. He, Z. Wei, F. Gao and J. Hou, *Adv. Mater.*, 2020, **32**, 1908205.
7 L. Liu, S. Chen, Y. Qu, X. Gao, L. Han, Z. Lin, L. Yang, W. Wang, N. Zheng, Y. Liang, Y. Tan, H. Xia and F. He, *Adv. Mater.*, 2021, 2101279.
8 F. Liu, L. Zhou, W. Liu, Z. Zhou, Q. Yue, W. Zheng, R. Sun, W. Liu, S. Xu, H. Fan, L. Feng, Y. Yi, W. Zhang and X. Zhu, *Adv. Mater.*, 2021, **33**, 2100830.
9 Y. Cai, Y. Li, R. Wang, H. Wu, Z. Chen, J. Zhang, Z. Ma, X. Hao, Y. Zhao, C. Zhang, F. Huang and Y. Sun, *Adv. Mater.*, 2021, 2101733.
10 X.-K. Chen and J.-L. Brédas, *Adv. Energy Mater.*, 2018, **8**, 1702227.
11 C.-M. Yang, C.-H. Wu, H.-H. Liao, K.-Y. Lai, H.-P. Cheng, S.-F. Horng, H.-F. Meng and J.-T. Shy, *Appl. Phys. Lett.*, 2007, **90**, 133509.
12 M. Qian, R. Zhang, J. Hao, W. Zhang, Q. Zhang, J. Wang, Y. Tao, S. Chen, J. Fang and W. Huang, *Adv. Mater.*, 2015, **27**, 3546–3552.
13 D. Veldman, S. C. J. Meskers and R. A. J. Janssen, *Adv. Funct. Mater.*, 2009, **19**, 1939–1948.
14 T. Basel, U. Huynh, T. Zheng, T. Xu, L. Yu and Z. V. Vardeny, *Adv. Funct. Mater.*, 2015, **25**, 1895–1902.
15 Y. Shao and Y. Yang, *Adv. Mater.*, 2005, **17**, 2841–2844.
16 J. Mei, K. Ogawa, Y.-G. Kim, N. C. Heston, D. J. Arenas, Z. Nasrollahi, T. D. McCarley, D. B. Tanner, J. R. Reynolds and K. S. Schanze, *ACS Appl. Mater. Interfaces*, 2009, **1**, 150–161.

17 G. L. Schulz and S. Holdcroft, *Chem. Mater.*, 2008, **20**, 5351–5355.
18 S.-L. Lai, L. Wang, C. Yang, M.-Y. Chan, X. Guan, C.-C. Kwok and C.-M. Che, *Adv. Funct. Mater.*, 2014, **24**, 4655–4665.
19 Z. Wan, J. Yang, Y. Liu, S. Wang, Y. Zhong, C. Li, Z. Zhang, G. Xing, S. Huettner and Y. Tao, *Polym. Chem.*, 2017, **8**, 4729–4737.
20 Z. Xue, S. Wang, J. Yang, Y. Zhong, M. Qian, C. Li, Z. Zhang, G. Xing, S. Huettner and Y. Tao, *npj Flexible Electron.*, 2018, **2**, 1–7.
21 S.-B. Li, Y. Geng and Z.-M. Su, *Org. Electron.*, 2020, **87**, 105956.
22 S.-B. Li, Y.-A. Duan, Y. Geng, H.-B. Li, J.-Z. Zhang, H.-L. Xu, M. Zhang and Z.-M. Su, *Phys. Chem. Chem. Phys.*, 2014, **16**, 25799–25808.
23 Z.-W. Zhao, Q.-Q. Pan, Y. Geng, S.-X. Wu, M. Zhang, L. Zhao and Z.-M. Su, *Org. Electron.*, 2018, **61**, 46–55.
24 L.-N. Wu, M.-Y. Sui, S. Xiao, Y.-Z. Xie and G.-Y. Sun, *Phys. Chem. Chem. Phys.*, 2020, **22**, 4015–4022.
25 M. J. Frisch, G. W. Trucks, H. B. Schlegel, G. E. Scuseria, M. A. Robb, J. R. Cheeseman, G. Scalmani, V. Barone, B. Mennucci, G. A. Petersson, H. Nakatsuji, M. Caricato, X. Li, H. P. Hratchian, A. F. Izmaylov, J. Bloino, G. Zheng, J. L. Sonnenberg, M. Hada, M. Ehara, K. Toyota, R. Fukuda, J. Hasegawa, M. Ishida, T. Nakajima, Y. Honda, O. Kitao, H. Nakai, T. Vreven, J. A. Montgomery Jr, J. E. Peralta, F. Ogliaro, M. Bearpark, J. J. Heyd, E. Brothers, K. N. Kudin, V. N. Staroverov, R. Kobayashi, J. Normand, K. Raghavachari, A. Rendell, J. C. Burant, S. S. Iyengar, J. Tomasi, M. Cossi, N. Rega, J. M. Millam, M. Klene, J. E. Knox, J. B. Cross, V. Bakken, C. Adamo, J. Jaramillo, R. Gomperts, R. E. Stratmann, O. Yazyev, A. J. Austin, R. Cammi, C. Pomelli, J. W. Ochterski, R. L. Martin, K. Morokuma, V. G. Zakrzewski, G. A. Voth, P. Salvador, J. J. Dannenberg, S. Dapprich, A. D. Daniels, O. Farkas, J. B. Foresman, J. V. Ortiz, J. Cioslowski and G. D. J. Fox, *Revision A.02*, Gaussian, Inc., Wallingford CT, 2009.
26 A. Perrier, F. Maurel and D. Jacquemin, *Acc. Chem. Res.*, 2012, **45**, 1173–1182.
27 C. Adamo and D. Jacquemin, *Chem. Soc. Rev.*, 2013, **42**, 845–856.
28 C. Leng, H. Qin, Y. Si and Y. Zhao, *J. Phys. Chem. C*, 2014, **118**, 1843–1855.
29 T. Yanai, D. P. Tew and N. C. Handy, *Chem. Phys. Lett.*, 2004, **393**, 51–57.
30 Y. Z. Li, T. Pullerits, M. Y. Zhao and M. T. Sun, *J. Phys. Chem. C*, 2011, **115**, 21865–21873.
31 I. Ciofini, T. Le Bahers, C. Adamo, F. Odobel and D. Jacquemin, *J. Phys. Chem. C*, 2012, **116**, 11946–11955.
32 D. Jacquemin, T. L. Bahers, C. Adamo and I. Ciofini, *Phys. Chem. Chem. Phys.*, 2012, **14**, 5383–5388.
33 T. Lu and F. Chen, *J. Comput. Chem.*, 2012, **33**, 580–592.
34 T. Lu, *Multiwfn, Version 3.3.8, A Multifunctional Wavefunction Analyzer*, available at, https://multiwfn.codeplex.com.
35 C. Risko, M. D. McGehee and J.-L. Bredas, *Chem. Sci.*, 2011, **2**, 1200–1218.
36 Y. Li, *Acc. Chem. Res.*, 2012, **45**, 723–733.
37 L. Zhang, K. Pei, M. Yu, Y. Huang, H. Zhao, M. Zeng, Y. Wang and J. Gao, *J. Phys. Chem. C*, 2012, **116**, 26154–26161.
38 H.-Y. Chen, J. Hou, S. Zhang, Y. Liang, G. Yang, Y. Yang, L. Yu, Y. Wu and G. Li, *Nat. Photonics*, 2009, **3**, 649–653.
39 S. D. Dimitrov and J. R. Durrant, *Chem. Mater.*, 2013, **26**, 616–630.
40 B.-G. Kim, X. Ma, C. Chen, Y. Ie, E. W. Coir, H. Hashemi, Y. Aso, P. F. Green, J. Kieffer and J. Kim, *Adv. Funct. Mater.*, 2013, **23**, 439–445.
41 D. Mühlbacher, M. Scharber, M. Morana, Z. Zhu, D. Waller, R. Gaudiana and C. Brabec, *Adv. Mater.*, 2006, **18**, 2884–2889.
42 G. D. Sharma, P. Balraju, J. A. Mikroyannidis and M. M. Stylianakis, *Sol. Energy Mater. Sol. Cells*, 2009, **93**, 2025–2028.
43 J. A. Mikroyannidis, S. S. Sharma, Y. K. Vijay and G. D. Sharma, *ACS Appl. Mater. Interfaces*, 2009, **2**, 270–278.
44 S.-C. Yiu, P.-Y. Ho, Y.-Y. Kwok, X. He, Y. Wang, W.-H. Yu, C.-L. Ho and S. Huang, *Chem.–Eur. J.*, 2022, DOI: 10.1002/chem.202104575.
45 D. Niedzialek, I. Duchemin, T. B. de Queiroz, S. Osella, A. Rao, R. Friend, X. Blase, S. Kümmel and D. Beljonne, *Adv. Funct. Mater.*, 2015, **25**, 1972–1984.
46 P. K. Samanta, D. Kim, V. Coropceanu and J.-L. Brédas, *J. Am. Chem. Soc.*, 2017, **139**, 4042–4051.
47 Y. L. Lin, M. A. Fusella and B. P. Rand, *Adv. Energy Mater.*, 2018, **8**, 1702816.
48 X. Liu, R. He, W. Shen and M. Li, *J. Power Sources*, 2014, **245**, 217–223.
49 B. Yang, Y. Yi, C. Zhang, S. G. Aziz, V. Coropceanu and J. Brédas, *J. Phys. Chem. C*, 2014, **118**, 27648–27656.
50 C. Keavney, R. Walters and P. Drevinsky, *J. Appl. Phys.*, 1993, **73**, 60–70.
51 C.-S. Jiang, H. Moutinho, D. Friedman, J. Geisz and M. Al-Jassim, *J. Appl. Phys.*, 2003, **93**, 10035–10040.
52 T. Stein, L. Kronik and R. Baer, *J. Am. Chem. Soc.*, 2009, **131**, 2818–2820.
53 X. Zhang, L. Chi, S. Ji, Y. Wu, P. Song, K. Han, H. Guo, T. D. James and J. Zhao, *J. Am. Chem. Soc.*, 2009, **131**, 17452–17463.
54 I. Constantinou, X. Yi, N. T. Shewmon, E. D. Klump, C. Peng, S. Garakyaraghi, C. K. Lo, J. R. Reynolds, F. N. Castellano and F. So, *Adv. Energy Mater.*, 2017, **7**, 1601947.